*The Nucleus* ***52****, No. 4 (2015) 180-184*

*www.thenucleuspak.org.pk*

**The Nucleus**

**ISSN 0029-5698 (Print)**

**ISSN 2306-6539 (Online)**

# Enhanced Photolumincence and Electrochemical Performance of ZnO/ZnS Coaxial Nanocables

M. Ahmad[1]*, H. Sun[2], A. Nisar[1], K. Maaz[1], G. Ali and S. Karim[1]

[1]*Nanomaterials Research Group, Physics Division, Directorate of Science, PINSTECH, Islamabad, Pakistan*

[2]*Beijing National Center for Electron Microscopy, Laboratory of Advanced Materials and the State Key Laboratory of New Ceramics and Fine Processing, Department of Materials Science and Engineering, Tsinghua University, Beijing, China*

*mashkoorahmad2003@yahoo.com; chempk@gmail.com; maaz@impcas.ac.cn; skarim73@gmail.com*

ARTICLE INFO

*Article history* :
*Received : 15 August, 2015*
*Revised : 04 November, 2015*
*Accepted : 13 December, 2015*

*Keywords* :
*ZnO,*
*ZnS,*
*Nanocable,*
*Lithium storage*

ABSTRACT

*ZnO based sulfide coaxial nanocables have been prepared by a two-step hydrothermal approach for the investigation of lithium storage capacity. The as-prepared ZnO/ZnS structures are analyzed by X-ray diffraction (XRD), scanning electron microscope (SEM), transmission electron microscopy (TEM), X-ray photospectroscopy (XPS), photoluminescence (PL) and by electrochemical work station. It has been found that these nanostructures demonstrate higher initial discharge capacity of 1096 mAhg$^{-1}$ with a 69% coulombic efficiency at a rate of 120 mAhg$^{-1}$ between 2 to 0.02 V. In addition, ZnO/ZnS structures show a significantly improved photoluminescence performance as compare with pure ZnO NWs. The enhanced lithium storage capacity and PL performance is ascribed to the coaxial structure of both materials.*

## 1. Introduction

Lithium-ion batteries (LIBs) are considered one of the most promising power sources for portable electronic devices such as electric vehicles and implantable medical devices due to their long cycle life, high energy capacity, and low environment impact etc. Nanostructured materials are capable of increasing the active reaction sites and accelerate the electron/Li ion transport [1-2]. Therefore, a lot of effort has been done to explore the Li storage capability of various nanostructures. Various 1D nanostructures, such as nanowires, nanobelts and nanocables have been fabricated by different methods [3]. Among them, coaxial nanocables consisting of a core and shell of different component materials may exhibit combined or distinctive properties. Up till now, InAs/InP, GaAs/GaP, TiO2/SnO2, Si/SiGe and ZnO/CdS nanocables have been synthesized by various methods including laser-assisted catalytic growth, metal organic chemical vapour deposition (MOCVD), thermal evaporation and sonochemical and chemical reaction [4]. However, there are few strategies for the effective and reliable production of coaxial nanocables.

Zinc oxide (ZnO) has a wide range of applications such as solar cell, batteries and medical devices due to its distinctive optical, electrical and electrochemical properties [5]. The use of ZnO nanostructures as electrode material for next generation rechargeable lithium-ion batteries has been much studied [6-10]. As an anode material ZnO has a theoretical capacity of 987 mAhg$^{-1}$, higher than that of commercialized graphite carbon (372 mAhg$^{-1}$). However, significant morphological changes during the formation of the Li-Zn alloys results in the deterioration of the electrode and poor cyclability of ZnO [11]. On the other hand, the sulfides including CdS and ZnS have been recently studied widely owing to the optoelectronic potential applications. Nanocomposites of 1D ZnO and sulfides may exhibit highly-enhanced LIBs properties [12].

Many efforts have been conducted to enhance the lithium storage capacity of anode materials by preparing nanostructure film electrodes, coating with Ni nanoparticles, or carbon layers, core-shell nano composites, junction formation, doping with some metals and so on. Among these efforts, morphology control is an effective way to overcome such problems.

## 2. Experimental

### *2.1 Materials*

Zinc sheet (99.9%), thioacetamide ($C_2H_5NS$) and hydrogen peroxide ($H_2O_2$) was purchased from Sinopharm Chemical Reagent Co., Ltd. Sodium hydroxide (NaOH) was purchased from Beijing Modern Eastern Fine Chemical. All chemical were of analytical grade and used without any further purification. All solutions used during the experiments were prepared using deionized water.

* Corresponding author

### 2.2 Synthesis

ZnO based sulfide coaxial nanocables were synthesized on the Zn substrate by a two step procedure. In the first step, hydrothermal technique was used to synthesize arrays of ZnO nanowire on a Zn substrate. Here, 10 mL of 2M NaOH and 5 mL of 30% $H_2O_2$ solution are mixed together under vigorous stirring and transferred to a stainless steel Teflon-lined autoclave of 20 mL volume. Subsequently, a zinc sheet piece is immersed in the above prepared solution. The autoclave is sealed and maintained at 180 $^oC$ for 12 h before being cooled down to room temperature. Then the zinc piece is removed from the solution, washed repeatedly with distilled water/ethanol and finally dried in for 2 h. In the second step, 0.56g of 0.15M thioacetamide ($C_2H_5NS$) solution was prepared in 50 ml distilled water and poured into the 100 mL stainless steel teflon-lined autoclave. The Zn piece from the first synthesis step is transferred into the autoclave before sealing. The reactor is maintained at 80 $^oC$ for 5 h before being cooled down to room temperature. After that, the final product is taken out from the solution and washed with distilled water, ethanol.

### 2.3 Apparatus

Field emission scanning electron microscopy (FESEM, JEM-6301F), transmission electron microscopy (TEM, Tecnai G20), and high resolution TEM (JEM-2011F) was used to investigate the morphology and microstructure of the product. The purity of phase were examined on a Bruker Model D8 Advance X-ray powder diffractometer (XRD) employing Cu Kα irradiation (λ = 1.5418 Å). Photoluminescence (PL) measurement was carried out at room temperature using the 325 nm line of the He-Cd laser with 1 kW/cm$^2$ excitation power using luminescence spectrometer (Hitachi F-4500).

### 2.4 Assembly of Cell

CR2032 coin cells were assembled in an argon glove box to perform electrochemical tests. The working electrode was fabricated by casting slurry onto a copper file and composed of 80 wt% active material (ZnO/ZnS NWs or pure ZnO NWs), 10 wt% polyvinylidene fluoride (PVDF), and 10 wt% carbon black. The 1M LiPF6 electrolyte was dissolved in a 1:1 (volume ratio) mixture of ethylene carbonate (EC) and diethyl carbonate (DMC). A lithium metal foil was used as the counter electrode. A glass fiber was used as a separator. A same CR2032 coin cell with the pure ZnO structure as the working electrode was assembled for the comparative study.

## 3. Results and Discussion

### 3.1 Morphological and Structural Characteristics

XRD patterns of the ZnO/ZnS and pure ZnO samples are presented in Fig. 1. All the peaks can be well assigned to those of wurtzite (hexagonal) ZnO/ZnS with lattice constants of a = 0.382nm and c = 0.626 nm (JCPDS: 36-1450) and wurtzite (hexagonal) ZnO, with lattice constants a = 0.325 nm and c = 0.521 nm (JCPDS: 36-1451). The Zn peaks in the pattern originate from the Zn substrate.

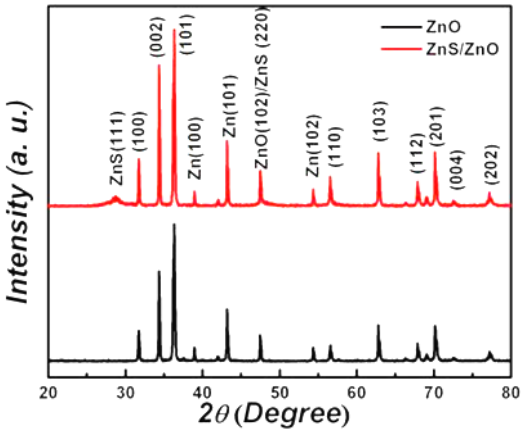


Fig. 1: XRD pattern of the ZnO/ZnS (Red line) and pure ZnO (Black line) samples

An image taken by SEM of pure ZnO sample is displayed in Fig. 2a. This displays that the product mainly consists of oriented arrays of NWs distributed uniformly on the Zn substrate. The wires are tens of micrometers long with diameters in the range of 100–200 nm. The morphology of the thioacetamide treated ZnO NWs sample consists of ZnO based sulfide coaxial nanocables as shown in Fig. 2b. The magnified SEM image of sulfide coaxial nanocables shown in the inset reveals that NWs maintain the morphology after thioacetamide treatment. It can be clearly seen that a sulfur layer is produced on the ZnO NWs with the tip of NW being buried. As compared to the pure ZnO NWs, the surface of the ZnO/ZnS nanocables is rough. The inset in Fig. 2b shows the EDS spectrum of the ZnO/ZnS nanocable. The EDS spectrum from coaxial cable exhibits the existence of S and Zn, together with a small percentage of O as compare with pure ZnO.

Figs. 2c and 2d are the low magnified TEM images of the ZnO/ZnS coaxial cable. It can be clearly seen that a uniform sulfur layer is deposited on the both sides of the ZnO NW. The contrast in the center part of the NW can be seen in Fig. 2d, confirms that the ZnS wraps the NW. Figs. 2e and 2f are the HRTEM images taken from the interface part of the ZnO/ZnS coaxial cable and clearly displays the ZnO and ZnS structure with different contrast. The selected area electron diffraction pattern (SAED) taken from both ZnS and ZnO confirms that the nanostructures are single crystals.

The oxidation state of the sulfur in the ZnO/ZnS coaxial cable has been analyzed by XPS analysis. The high resolution XPS spectra of S2p, Zn3p and O1s peaks are shown in Fig. 3(a-c). In Fig. 3c, the peak at binding

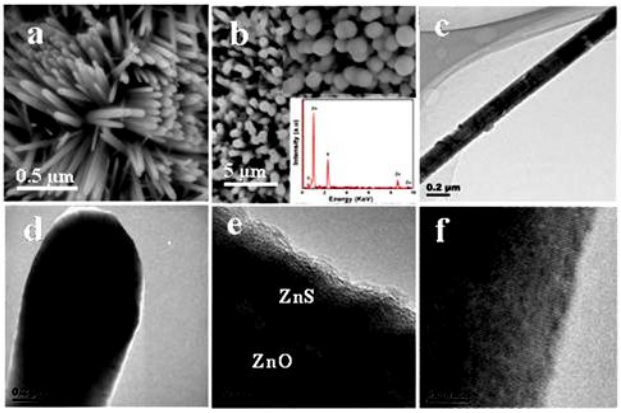


Fig. 2: SEM images of (a) pure ZnO NWs (b) Coaxial ZnO/ZnS NWs; Inset is the corresponding EDS (c) & (d) TEM images of coaxial ZnO/ZnS NWs (e) & (f) HRTEM images of ZnO/ZnS NWs from the interface region

energy 530.4 and 531.7 eV are ascribed to lattice oxygen in the coaxial structure. The spectrum in Fig. 3a shows that the two significant peaks at the binding energies of 161.6 and 162.5 eV could be assigned to S2p3/2 and S2p1/2 respectively. The S2p peak in the spectrum clearly indicates the existence of S element in coaxial cable. Two significant peaks shown in Fig. 3b corresponding to Zn2p3/2 and Zn2p1/2 located at the binding energies of 1020.8 and 1043.2 eV, respectively. These results are in good agreement with the previous reports [13] and confirm the coaxial cable structure of ZnO/ZnS.

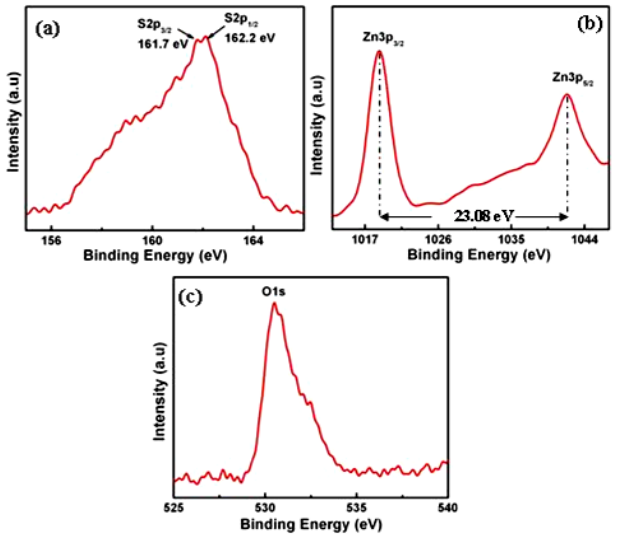


Fig. 3: XPS spectra of (a) S2p (b) Zn3p and (c) O1s

Fig. 4 shows room temperature PL spectra of both ZnO and ZnO/ZnS coaxial structure. In the ZnO spectrum, a UV peak at 381.4 nm and a broad green emission band between 470-700 nm is present. While, in comparison, the ZnO/ZnS structure shows a strong UV emission peak at 378.8 nm and a weak wide green

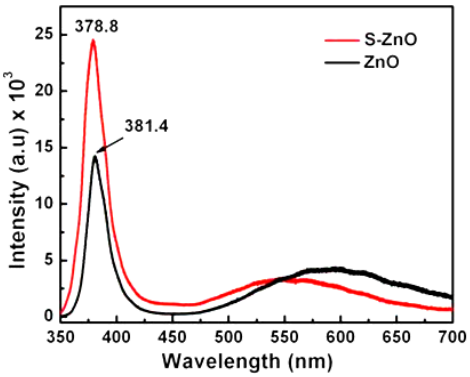


Fig. 4: Room temperature PL spectra of ZnO NWs and ZnO/ZnS coaxial structure

emission centered at 550 nm. In accordance with the reference 14, self-activated centers, such as the singly ionized charge state of specific defects, oxygen vacancies, and elemental sulfur atoms vacancy originating from the lattice mismatch between ZnS and ZnO at the interface region results in the green emission [14]. The peak position of coaxial structure shows a blue-shift of about 23 nm in contrast to ZnO. This blue-shift is due to the sulfur incorporation and ZnO/ZnS interfaces in the structure, as discussed in the literature [15]. The increase in UV emission could be attributed to the good quality of coaxial cables.

### 3.2 *Electrochemical Application*

The cyclic voltammogarms of ZnO/ZnS coaxial cable based electrode at a scan rate of 0.5 $mVs^{-1}$ are shown in Fig. 5a. In the first scanning cycle, the cathodic peak with maximum intensity at 0.34 V starts at 0.22 V. This can be ascribed to the decomposition of zinc sulfide into metallic Zn and the formation of $Li_2S$ with the following reaction.

$$ZnS + 2Li^{+} \rightarrow Zn + Li_2 S \qquad (1)$$

Some of the electrolyte is consumed in the formation of passivated film (SEI) on the electrode surface. The formation of $Li_xZn$ alloy results in the broad cathodic peak between 0.51 to 1.14 V in the first cycle. The redox peak in the low voltage range is related to the reversible formation and decomposition of lithium zinc alloys. Lithiation products of $Li_xZn$ alloys and $Li_2S$ are present at the end of the cathodic scans. Three anodic peaks can be clearly observed during the anodic scan at 0.42 V, 0.58 and 0.74 V vs. $Li/Li^{+}$, respectively. Lithium ions are extracted from $Li_xZn$ alloys in the anodic scan to generate $Li^{+}$ and Zn in the low voltage range. ZnS is regenerated in a fully charged state with increasing scanning potential and that is the reason for the anodic peak at 1.4 V. CV curves exhibit no peak shape change in the subsequent cycles representing thus a high reversibility of the coaxial nanocable electrode. The following reactions take place during the anodic scan :

$$Li_xZn \rightarrow Li^+ Zn \quad (2)$$

$$Zn + Li_2S \rightarrow ZnS + Li^+ \quad (3)$$

The potential range of 0–2 V vs Li/Li$^+$ is suitable for the charge – discharge cycling as evident in the CV response which shows that the anodic peaks appear in the range of 0.22–1.40 V vs Li/Li$^+$. Thus CV behavior confirms that both the ZnO and ZnS in the coaxial nanocable structure are electrochemically active materials for lithium storage.

Fig. 5b represents the galvanostatic discharge-charge capacity curve for the ZnO/ZnS coaxial nanocable and pure ZnO NWs electrodes in the voltage range of 3–0.02 V at a current density of 120 mAg$^{-1}$. It shows that the voltage profiles of the ZnO/ZnS coaxial nanocable electrode drops rapidly and reaches a plateau at ~ 0.4 V during the first discharge and then followed by slop down to 0.01 V. Fig. 5b shows that the ZnO/ZnS coaxial nanocable electrode exhibit an initial discharge capacity of about 1540 mAhg$^{-1}$ and coulombic efficiency of 69 % which is higher than that of pure ZnO electrode. The improved lithium storage capacity of ZnO/ZnS nanostructure cell might result from the Li activity of Zn-S phase.

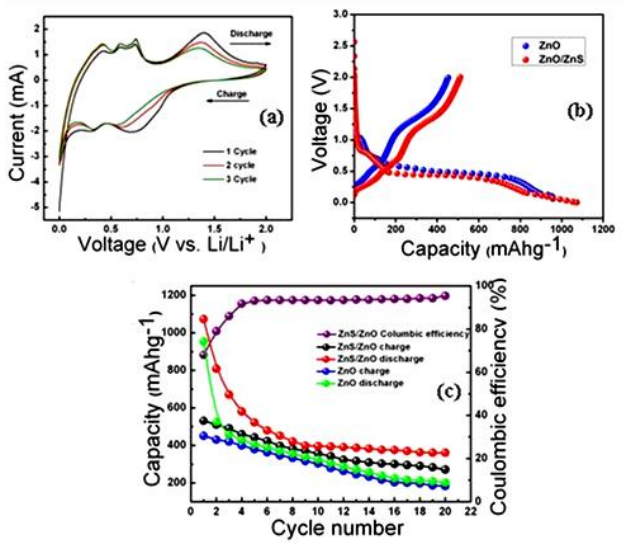


Fig. 5: (a) Cyclic voltammetery sweep curve (CV) of the electrode ; (b) Galvanostatic charge/discharge curves of the coaxial electrode at a voltage range of 0.02-3.0V (c) capacity and Coulombic efficiency of the cell vs. cycle number for the ZnO/ZnS film electrode

The comparison of the cycling performance of ZnO/ZnS and ZnO cells at a current density of 120 mAhg$^{-1}$ is shown in Fig. 5c. It can be observed that the discharge capacity of the ZnO/ZnS coaxial nanocable based cell decreases to 811 mAhg$^{-1}$ after second cycle and 525 mAhg$^{-1}$ after fifth cycle. The degradation is slower in subsequent cycles and a stable capacity of 402 mAhg$^{-1}$ reach after 15 cycles. A stable reversible capacity of 368 mAhg$^{-1}$ is obtained after the cell is cycled for 20 cycles which is still higher than the theoretical capacity of graphite. In contrast, the capacity of the ZnO electrode decays rapidly to 322 mAhg$^{-1}$ after 10 cycles between 2 and 0.02 V as shown in Fig. 5c. The improved capacity and cycle life of the ZnO/ZnS coaxial nanocable electrode can be attributed to the ZnO/ZnS coaxial nanocable structure, which provide better accommodation of the large volume change during lithiation/delithiation process. The ZnO/ZnS coaxial nanocable facilitates the diffusion of lithium ions and may provide greater accessibility to the active sites for subsequent alloy and de-alloy processes [16].

The morphological changes during cell operation are also recorded for both the nanostructures by taking micrographs by SEM and TEM after 20 cycles and it was found that the ZnO/ZnS coaxial nanocable preserve the morphology (not shown here). While ZnO structure morphology change after 10 cycles. The preservation of ZnO/ZnS structure during the Li$^+$ insertion/extraction process results in to keep the strong electrical interaction between ZnS and ZnO thus improving the stability of cycling.

## 4. Conclusions

In summary, two-step hydrothermal process has been used to synthesize ZnO/ZnS coaxial structures which are found to be a promising anode material for rechargeable lithium ion battery. This novel nanostructured material shows enhanced lithium storage capacity with good cycling performance and high coulombic efficiency. The improved performance is mainly due to the ZnS nanostructure which acts as good electronic conductors. From our results there are the possibilities to produce highly-efficient anode materials for lithium ion batteries that show high reversible capacity. In future, this method can be utilized to produce innovative ZnO/ZnS junctions to explore more applications.

## References

[1] P. Poizot, S. Laruelle, S. Grugeon, L. Dupont and J.-M. Tarascon, “Nano-sized transition-metal oxides as negative-electrode materials for lithium-ion batteries”, Nature, vol. 407, pp. 496-499, September 2000.

[2] A.S. Arico, P. Bruce, B. Scrosati, J.-M. Tarascon and W. Vn Schalkwijk, “Nanostructured materials for advanced energy conversion and storage devices”, Nature Mater., vol. 4, pp. 366-377, May 2005.

[3] M. Ahmad and J. Zhu, “ZnO based advanced functional nanostructures: synthesis, properties and applications”, J. Mater. Chem., vol. 21, pp. 599-614, September 2011.

[4] M. Ahmad, J. Zhao, J. Iqbal, W. Miao, L. Xie, R. Mo, and J. Zhu, “Conductivity enhancement by slight indium doping in ZnO nanowires for optoelectronic applications”, J. Phys. D: Appl. Phys., vol. 42, pp. 165406-165412, July 2009.

[5] M. Ahmad, C. Pan, and J. Zhu, “Electrochemical determination of L-Cysteine by an elbow shaped, Sb-doped ZnO nanowire-modified electrode”, J. Mater. Chem., vol. 20, pp. 7169-71714, July 2010.

[6] C. Q. Zhang, J. P. Tuz, Y. F. Yuan, X. H. Huang, X. T. Chen and F. Mao "Electrochemical performances of Ni-coated ZnO as an anode material for lithium-ion batteries", J. Electrochem. Soc., vol. 154, pp. A65-A69, December 2007.

[7] G.F. Yan, H.S. Fang, G.S. Li, L.P. Li, H.J. Zhao and Y. Yang, "Improved electrochemical performance of Mg-doped ZnO thin film as anode material for lithium ion batteries", Chinese J. Struct. Chem., vol. 28, no. 4, pp. 409−413, 2009.

[8] J. Liu, Y. Li, X. Huang, G. Li and Z. Li, "Layered double hydroxide nano- and microstructures grown directly on metal substrates and their calcined products for application as Li-ion battery electrodes", Adv. Func. Mater. vol. 18, pp. 1448-1458, April 2008.

[9] M. Ahmad, S. Yingying, A. Nisar, H. Sun, W. Shen, M. Wei and J. Zhu, "Synthesis of hierarchical flower-like ZnO nanostructures and their functionalization by Au nanoparticles for improved photocatalytic and high performance Li-ion battery anodes", J. Mater. Chem., vol. 21, pp. 7723-7729, April 2011.

[10] J. Liu, Y. Li, R. Ding, J. Jiang, Y. Hu, X. Ji, Q. Chi, Z. Zhu and X. Huang, "Carbon/ZnO nanorod array electrode with significantly improved lithium storage capability", J. Phys. Chem., vol. C 113, pp. 5336-5339, March 2009.

[11] Y. Yu, C.-H. Chen, J-L. Shui and S. Xie, "Nickel-foam-supported reticular CoO–Li2O composite anode materials for lithium ion batteries", Angew. Chem., Int. Ed., vol. 44, pp. 7085-7089, November 2005.

[12] Y. Idota, T. Kubota, A. Matsufuji, Y. Maekawa and T. Miyasaka, "Tin-based amorphous oxide: A high-capacity lithium-ion-storage material", Science, vol. 276, 1395-1397, May 1997.

[13] M. Ahmad, X. Yan, and J. Zhu, "Controlled synthesis, structural evolution, and photoluminescence properties of nanoscale one-dimensional hierarchical ZnO/ZnS heterostructures", J. Phys. Chem., vol. C 115, pp. 1831-1837, January 2011.

[14] H. Zheng, G. Duan, Y. Li, S. Yang, X. Xu, W. Cai, "Blue luminescence of ZnO nanoparticles based on non-equilibrium processes: Defect origins and emission controls", Adv. Funct. Mater., vol. 20, pp. 561-572, February 2010.

[15] H. Peng, B. Liuyang, Y. Lingjie, L. Jinlin, Y. Fangli, C. Yunfa, "Shape-controlled synthesis of ZnS nanostructures: A simple and rapid method for one-dimensional materials by plasma", Nanoscale Res Lett., vol. 4, pp. 1047-1053, June 2009.

[16] C.-Ho Lai, M.-Yen Lu and L. Juann Chen, "Metal sulfide nanostructures: synthesis, properties and applications in energy conversion and storage", J. Mater. Chem., vol. 22, pp. 19-30, November 2012.